# Fast Electron Transport in Ultraintense Laser Pulse Interaction with Solid Targets by Rear-Side Self-Radiation Diagnostics

J. J. Santos,[1] F. Amiranoff,[1] S. D. Baton,[1] L. Gremillet,[1] M. Koenig,[1] E. Martinolli,[1] M. Rabec Le Gloahec,[2]
C. Rousseaux,[2] D. Batani,[3] A. Bernardinello,[3] G. Greison,[3] and T. Hall[4]
[1]*Laboratoire pour l'Utilisation des Lasers Intenses, UMR7605, CNRS-CEA-Université Paris VI-Ecole Polytechnique, 91128 Palaiseau, France*
[2]*Commissariat à l'Energie Atomique, 91680 Bruyères-le-Châtel, France*
[3]*Dipartimento di Fisica G. Ochialini, Università degli Studi di Milano-Bicocca and INFM, P.za Scienza 3, 20126 Milan, Italy*
[4]*University of Essex, Colchester CO4 3SQ, United Kingdom*
(Received 26 February 2002; published 24 June 2002)

We report on rear-side optical self-emission results from ultraintense laser pulse interactions with solid targets. A prompt emission associated with a narrow electron jet has been observed up to aluminum target thicknesses of 400 $\mu$m with a typical spreading half-angle of 17°. The quantitative results on the emitted energy are consistent with models where the optical emission is due to transition radiation of electrons reaching the back surface of the target or due to a synchrotron-type radiation of electrons pulled back to the target. These models associated with transport simulation results give an indication of a temperature of a few hundred keV for the fast-electron population.

DOI: 10.1103/PhysRevLett.89.025001 PACS numbers: 52.50.Jm, 52.38.Ph, 52.70.Kz

In the fast igniter scheme, an alternative to classical inertial confinement fusion where fuel compression and ignition are dissociated [1,2], fuel heating and ignition would be achieved by energy deposition of a fast-electron jet. Limiting aspects of the classical approach such as implosion symmetry and drive energy are expected to be considerably relaxed. The relativistic electron jet is generated by an ultraintense and ultrashort laser pulse interacting with the ablated plasma in the neighborhood of its critical density ($n_c$). Fast-electron transport over a distance of about 300 $\mu$m from this moderately dense region till the compressed fuel ($\sim 1000 n_c$) is then a crucial issue for the success of the scheme.

Several experiments have already produced interesting results within the framework of fast-igniter and fast-electron transport into dense, either solid [3–7] or shock compressed matter [8–10], shedding some light on laser/electron energy conversion efficiency, hot electron penetration range, material stopping power, and transport inhibition by electric field. Also the observation of very collimated high-intensity laser-produced electron jets traveling through solid insulator targets has been reported previously [11,12]. Nevertheless precise measurements of the spatial and temporal evolution of the fast-electron beam inside the target and of the induced target heating, critical for the ignition efficiency, has still to be performed. In this Letter, we present results on time-integrated and time-resolved Al targets' rear-side optical self-emission. A prompt emission giving evidence of fast electrons reaching the rear surface has been observed. The narrow, bright, and very brief ($\sim$ps) structure spreads with a half-angle of $\simeq 17°$ and becomes progressively less intense with target thickness up to 400 $\mu$m.

The experiment was performed at the LULI 100 TW laser facility. A 350 fs, 1.057 $\mu$m laser pulse with an energy up to 10 J on target was focused by a $f/3$ off-axis parabola at normal incidence onto Al flat targets with thicknesses ranging from 17 to 400 $\mu$m. From both low-intensity focal spot measurements and x-ray pinhole pictures obtained with the same target irradiation setup, the laser focal spot is measured to be less than 20 $\mu$m FWHM, corresponding to a maximum laser intensity of $10^{19}$ W cm$^{-2}$.

The target rear side was imaged by means of a $f/2$ optical system on both a CCD camera and a streak camera, as shown in Fig. 1. The time-integrated images were obtained with a 1024 × 1024 12-bit CCD camera and the time-resolved ones with a Hadland S20 streak camera, coupled to a 512 × 512 12-bit CCD camera. A spatial resolution of a few $\mu$m was obtained. The time resolution depended on the chosen sweep speed and slit width. These cameras were adequately filtered to suppress the undesirable 1.06 $\mu$m (2 mm KG3 filter) and 0.53 $\mu$m (two Kodak magenta filters) wavelengths from the probe beam used simultaneously on the target rear-side reflectivity diagnostic [13]. By taking into account the optics, all the filters, and camera responses, acquisition was possible in the spectral range between 370 and 880 nm, except for a 60 nm region around 530 nm.

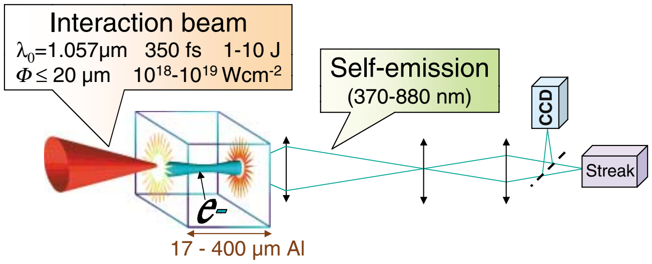

FIG. 1 (color online). Experimental setup.

0031-9007/02/89(2)/025001(4)$20.00

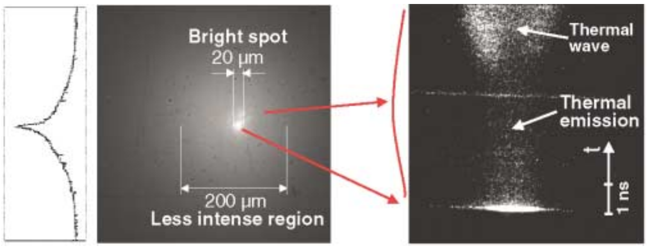

FIG. 2 (color online). Time-integrated and vertical lineout (on the left) and time-resolved (on the right) images of the self-emission from the rear surface of Al targets.

In Fig. 2 we present typical images obtained on both detectors. On the left, in a time-integrated image of a full energy shot (~10 J on target) onto a 35 $\mu$m target, we see a central narrow bright spot surrounded by a less intense region. A central lineout of this image is also shown. On the right is the time-resolved image of a moderate energy shot (~5 J on target) onto a 75 $\mu$m target. This result allowed us to distinguish two types of radiation: a first very short duration (less than 10 ps) and very intense signal, followed by a much less intense and long duration signal (few ns). The first one, to which corresponds the bright spot in the integrated image, is attributed to fast electrons reaching the target rear surface, whereas the second one is thought to evidence the thermal emission of the cooling and expanding plasma heated by the fast electrons and the associated mechanisms. The signal observed about 4.5 ns after the short signal is interpreted as the breakout of a thermal wave after burning through the target. These longer emissions correspond to the less intense and larger signal of the integrated image.

Using a larger slit and a faster sweep speed we have managed to freeze the first brief and intense signal. A series of snapshots of this prompt signal are shown in Fig. 3 for full energy shots and different target thicknesses from 35 up to 400 $\mu$m. These images correspond to the central bright spot of the integrated signals, allowing us to conclude that most of the radiation in the central bright spot is emitted during the first picoseconds and, therefore, that it is connected with the fast-electron jet crossing the target rear side. For increasing thicknesses, the width of the spot increases quasilinearly, showing an electron beam spread within the target of about 17° half-angle. The total energy smoothly decreases for target thickness larger than 100 $\mu$m, but a very rapid variation of the signal is observed between 35 and 75 $\mu$m (Fig. 4). In one experimental run, the measurements present a typical variation of about a factor of 4, probably connected to variations in the laser intensity profile or in the laser temporal profile. The total energy is given by an absolute calibration of the detection system with an uncertainty of a factor of 2–3.

In our experiment, the interaction laser pulse had an amplified spontaneous emission (ASE) low-intensity pedestal with a contrast in energy of $10^{-4}$ arriving 1.5 ns before the short part. From simulations performed with the hydrocode MULTI-FEMTO [14,15], the propagation of the ASE-induced shock wave is expected to take 4.5 ns to cross 17 $\mu$m of Al (the thinner target used), and should not consequently interfere with the fast-electron transport.

Several physical mechanisms could be responsible for the initial short signal: (i) optical transition radiation (OTR), which is light emitted when a charged particle crosses the boundary between two media with different dielectric properties [16]. (ii) Synchrotron-type radiation: the fast electrons leaving the material create a positive sheath potential that pulls them back within a distance of the order of the Debye length. Their "rotation" to reenter the target would be responsible for a synchrotronlike emission [17]. (iii) "Blackbody" thermal emission of the heated surface. Because of the very short duration of the signal ($\leq$10 ps), it is unlikely that the short signal is due to thermal radiation; in fact, for a measured target heating $\lesssim$30 eV from extreme violet (180 Å) imaging diagnostics, hydrodynamic expansion simulations predict a much longer time for the target to cool down after the rapid heating [18]. Also, the bremsstrahlung radiation from the electron propagation through matter has not been considered because of the spectral domain of our detection system.

For the first two mechanisms we calculated the energy conversion efficiency between the electron kinetic energy and the possible observed signal (taking into account the detection geometry, all the filters, and the absolute sensitivity). They are represented in Fig. 5 as a function of the electron kinetic energy and its outcoming angle (with respect to the symmetry axis of observation) in the OTR case, and as a function of electron kinetic energy and trajectory radii of curvature in the synchrotron case. In the OTR case, the maximum efficiency is obtained for high electron energies ($\gtrsim$2 MeV) leaving the target near normal incidence. The relativistic dipolelike emission is then collected by the imaging optics. At low electron energies

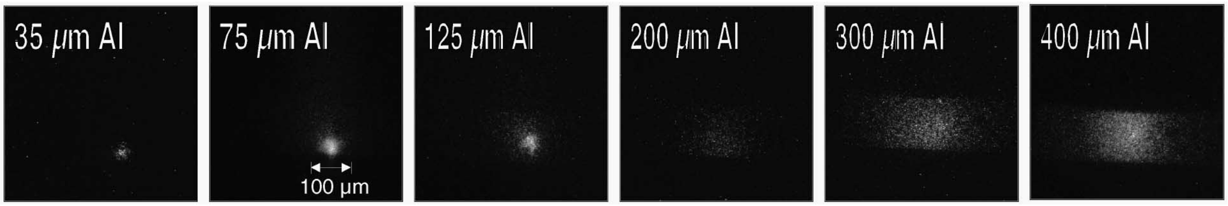

FIG. 3. Time-resolved snapshots of the self-emission from the rear side of Al targets with thicknesses ranging from 35 up to 400 $\mu$m. The laser energy on target was 10 J. Used neutral densities were, from left to right, ND = 3.5, 1, 1, 1, 0.5, 0.

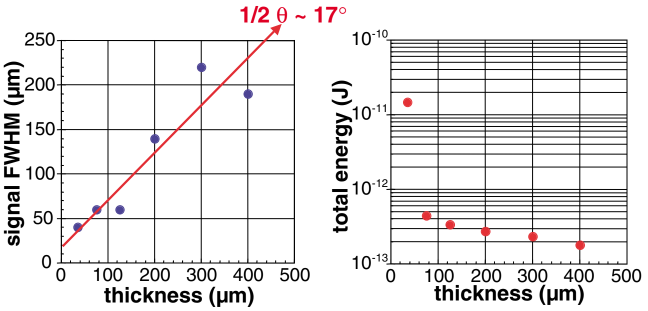

FIG. 4 (color online). Evolution of the initial short rear-side self-emission with target thickness from one series of full energy shots (10 J on target): spot FWHM (on the left) and integrated energy (on the right).

($\lesssim$500 keV), on the contrary, a significant amount of light is emitted near 0° only for large outgoing angles. In the synchrotron case we see that even the low-energy electrons can emit a significant fraction of the total detectable radiation. Another interesting feature is that, for radii larger than the observed wavelength, the efficiency becomes almost independent of the radius of curvature, presenting a tenuous oscillation pattern.

Numerical simulations of fast-electron transport into dense matter have been done with the 3D hybrid code PÂRIS [11,19,20]. This code models both collision effects (multiple scattering and slowing down) and self-generated magnetic and electric fields in a MHD approximation [21]. Simulation conditions for the initial electron population were chosen in order to be as close as possible to the experimental conditions. An incoming electron population with a total kinetic energy of 1.2 J is injected into the target in a region of 8 $\mu$m diameter and over a time duration of 300 fs. The temperature of the hot electrons injected into the target depends on space and time and is given by [22]

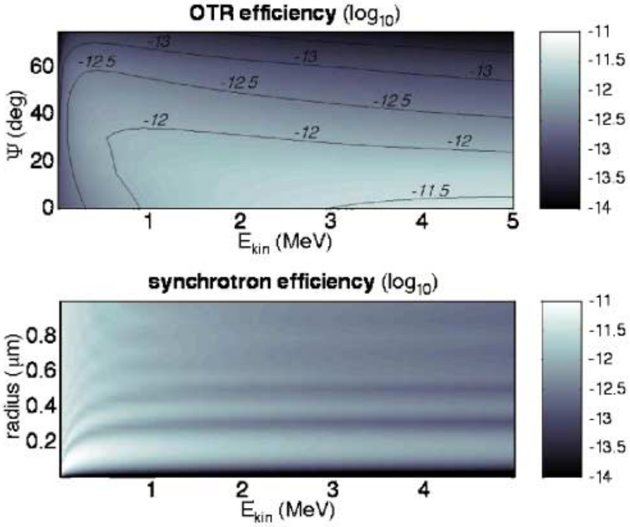

FIG. 5 (color online). Conversion efficiency (in $\log_{10}$) of electron kinetic energy into radiated energy. Dependence on electron kinetic energy and the outcoming angle is shown for the OTR case (upper image) and on electron kinetic energy and trajectory radii for the synchrotron case (lower image).

$$T_h(r,t) = 100[I_{17}(r,t)]^{1/3}\ [\mathrm{keV}], \tag{1}$$

where $I_{17}(r,t)$ is the laser intensity in units of $10^{17}$ W cm$^{-2}$. The initial electron energy distribution is a 1D relativistic Maxwellian function:

$$f_p(r,t) \propto \exp\left\{-\frac{E_0}{T_h(r,t)}[(1+p^2)^{1/2}-1]\right\}, \tag{2}$$

where $p$ is the electron momentum in units of $m_e c$ and $E_0 = 511$ keV. Its angular distribution with respect to the interaction axis is given by $df(\theta) \propto e^{-\theta^2/\theta_0^2}\sin\theta d\theta$. Considering the experimental results (see Fig. 4; [3,4]), we have chosen $\theta_0 = 20°$.

For these initial conditions and an Al propagation thickness of 75 $\mu$m, PÂRIS predicts that $2.8 \times 10^{12}$ electrons should reach the target rear side, which amounts to a total kinetic energy of 0.29 J. Taking into account the energy and angle of each electron on the back surface, the predicted total OTR signal is $4.0 \times 10^{-13}$ J. For the synchrotron case, we have taken the radial distribution of the electron surface density and mean kinetic energy ($T_h$) on the rear side. We have then estimated the corresponding maps of Debye length ($\lambda_D$) and electrostatic field ($E$) assuming $eE = k_B T_h/\lambda_D$. On the interaction axis the electrostatic field has a maximum value of $\sim$10 MV/$\mu$m. For each particle coming out, at a given position and with a given energy, we estimated the maximum distance it could reach and its radiated synchrotron light. For our experimental detection geometry, the total detected synchrotron energy is $4.9 \times 10^{-13}$ J. Thus, both the OTR and synchrotron models give radiated energies very close to the experimental value of $4.5 \times 10^{-13}$ J.

Because of excessive requirements on memory size, we could not use PÂRIS for target thicknesses larger then 100 $\mu$m. In order to assess the electron spreading in a wider range of thicknesses we have used instead the Monte Carlo collisional code PROPEL [19]. We injected 1D relativistic Maxwellian electron distributions for temperatures $T_h$ between 0.1 and 1 MeV [Eq. (2), independent on space and time], with a total energy of 1.2 J, into pure Al propagation layers with thicknesses ranging between 35 and 500 $\mu$m. Each particle was injected individually at normal incidence and within a spot radius of 10 $\mu$m.

We have applied the OTR efficiency (see Fig. 5) to the simulation electrons coming out of the rear side and confronted the corresponding OTR signal width and total energy with experimental data: In Fig. 6a we can see that, assuming a pure collisional transport, the experimental radial spread of the OTR signal as a function of target thickness is best fitted for $T_h = 0.3$–$0.5$ MeV. On the other hand, as regards the detectable OTR radiation energy level, we see in Fig. 6b that the closest fit for experimental

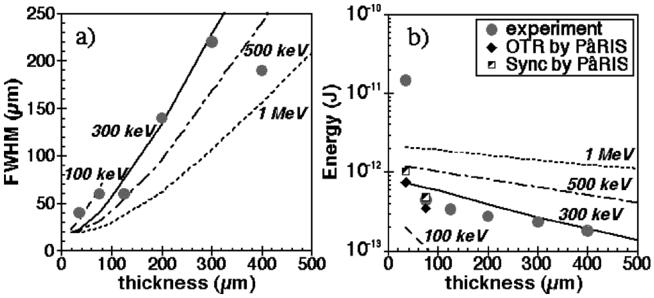

FIG. 6. OTR model applied to PROPEL simulations for different temperature electron populations (lines) compared to experiment: (a) signal radial spreading; (b) signal total energy. Expected OTR and synchrotron energy levels for PÂRIS simulations are also shown.

data corresponds to $T_h = 0.3$ MeV. However, this result depends on the initial electron kinetic energy of 1.2 J. Actually the slope for $T_h = 0.5$ MeV is the one that best describes the experimental energy decrease with target thickness. OTR and synchrotron energies obtained from PÂRIS simulations are also represented.

By comparing the results from PÂRIS and PROPEL for thin propagation layers, it seems that taking into account the electromagnetic response of the propagation medium (case of PÂRIS) produces a steeper signal evolution with target thickness, but still not enough to explain the experimental sudden drop of the signal beyond 35 μm. We can also see that a low component in the electron distribution (see fit for $T_h = 100$ keV) does not explain this result. If the slope of the curve is effectively much steeper, the fast-electron total energy consistent with the large signal would be an unreasonable 100 J.

Another possibility could be the circulative motion of electrons inside the target (refluxing): hot electrons are reflected at the target rear side by the sheath potential and reinjected into the target. If the target is thin enough, hot electrons reaching again the front side can be reinjected back into the dense region, yielding an overlap of the electron beams and an increase in the hot electron density. Moreover, if the electrons are still collimated within the laser focal spot when they reach the front side, they can be reaccelerated by a later part of the laser pulse, contributing to the formation of a hot tail in the electron distribution. This has been observed in particle-in-cell simulations for propagation layers thinner than a critical target thickness $L_c = L_p/2$, where $L_p$ is the laser pulse length [23].

In conclusion, we have measured the optical emission of the back surface of Al targets irradiated by intense and short laser pulses. A bright and short signal has been observed up to 400 μm thickness, being a geometrical signature of fast-electron jets crossing the target-vacuum boundary. The spread of the electron jet inside the target is $1/2\theta \approx 17°$, which fairly agrees with other results from x-ray or UV measurements [3,4,10]. Both optical transition radiation and synchrotron radiation models are energetically consistent with the experimental data, giving an indication of an electron population with a temperature of a few hundred keV, which is also in agreement with x-ray emission results [7].

We gratefully acknowledge J. C. Gauthier, T. E. Cowan, and Y. Sentoku for fruitful discussions, as well as the assistance of the LULI laser staff. This work was supported by the E.U. TMR Laser Facility Access Program (Contract No. ERBFMGE-CT95-0044) and in part by Grant No. E 1127 from Région Ile de France. One of us (J. J. S.) was financed by the MCT (Portugal) under Contract No. PRAXIS XXI BD/18108/98.

[1] M. Tabak *et al.,* Phys. Plasmas **1**, 1626 (1994).
[2] S. Atzeni, Jpn. J. Appl. Phys. **34**, 1980 (1995).
[3] M. H. Key *et al.,* Phys. Plasmas **5**, 1966 (1998).
[4] K. B. Wharton *et al.,* Phys. Rev. Lett. **81**, 822 (1998).
[5] M. Tatarakis *et al.,* Phys. Rev. Lett. **81**, 999 (1998).
[6] F. Pisani *et al.,* Phys. Rev. E **62**, R5927 (2000).
[7] J. A. Koch *et al.,* Phys. Rev. E **65**, 016410 (2001).
[8] T. A. Hall *et al.,* Phys. Rev. Lett. **81**, 1003 (1998).
[9] D. Batani *et al.,* Phys. Rev. E **61**, 5725 (2000).
[10] R. Kodama *et al.,* Nature (London) **412**, 798 (2001).
[11] L. Gremillet *et al.,* Phys. Rev. Lett. **83**, 5015 (1999).
[12] M. Borghesi *et al.,* Phys. Rev. Lett. **83**, 4309 (1999).
[13] E. Martinolli *et al.* (to be published).
[14] R. Ramis *et al.,* Comput. Phys. Commun. **49**, 475 (1988).
[15] K. Eidmann *et al.,* Phys. Rev. E **62**, 1202 (2000).
[16] I. Frank and V. Ginzburg, J. Phys. USSR **9**, 353 (1945).
[17] J. D. Jackson, *Classical Electrodynamics* (Wiley, New York, 1975), 2nd ed.
[18] M. H. Key *et al.,* in IFSA2001 Proceedings, Kyoto, Japan, 2001 (to be published).
[19] L. Gremillet, Ph.D. thesis, Ecole Polytechnique, France, 2001.
[20] L. Gremillet *et al.,* Phys. Plasmas **9**, 941 (2002).
[21] J. R. Davies *et al.,* Phys. Rev. E **59**, 6032 (1999).
[22] F. N. Beg *et al.,* Phys. Plasmas **4**, 447 (1997).
[23] A. J. Mackinnon *et al.,* Phys. Rev. Lett. **88**, 215006 (2002).